

1 A global survey of cloud overlap
2 based on CALIPSO and CloudSat measurements

3 Jiming Li,¹ Jianping Huang,^{1,*} Knut Stamnes,²

4 Tianhe Wang,¹ Qiaoyi Lv¹, Hongchun Jin¹

5 ¹Key Laboratory for Semi-Arid Climate Change of the Ministry of Education, College
6 of Atmospheric Sciences, Lanzhou University, Lanzhou, China

7 ²Department of Physics and Engineering Physics, Stevens Institute of Technology,
8 Hoboken, NJ, USA

9
10 Running Head: Statistical properties of cloud overlap

11
12 *Corresponding author: Jianping Huang, Key Laboratory for Semi-Arid Climate
13 Change of the Ministry of Education, College of Atmospheric Sciences, Lanzhou
14 University, Lanzhou, Gansu 730000, China. (hjp@lzu.edu.cn)

Abstract

Using 2B-CLDCLASS-Lidar (Radar-Lidar) cloud classification and 2B-FLXHR-LIDAR radiation products from CloudSat over four years, this study evaluates the co-occurrence frequencies of different cloud types, analyzes their along-track horizontal scales and radiative effects, and utilizes the vertical distributions of cloud types to preliminarily evaluate cloud-overlap assumptions.

The statistical results show that high clouds, altostratus, altocumulus and cumulus are much more likely to co-exist with other cloud types. However, stratus (or stratocumulus), nimbostratus and convective clouds are much more likely to exhibit individual features. On average, altostratus-over-stratus/stratocumulus cloud systems have a maximum horizontal scale (17.4 km), with a standard deviation of 23.5 km. altocumulus-over-cumulus has a minimum scale (2.8 km), with a standard deviation of 3.1 km. By considering the weight of each multilayered cloud type, we find that the global mean cloud radiative effects of multilayered cloud systems during the daytime are approximately -41.3 W/m^2 and -50.2 W/m^2 (a 41% radiative contribution) at the top of the atmosphere (TOA) and at the surface, respectively. The radiative contributions of high-over-altocumulus and high-over-stratus/stratocumulus (or cumulus) to the entire multilayered cloud system are dominant due to their frequency.

Considering the overlap of cloud types, the cloud fraction based on the random overlap assumption is underestimated over vast oceans, except in the west-central Pacific Ocean warm pool. Obvious overestimations mainly occur over tropical and subtropical land masses. In view of an lower degree of overlap than that predicted by the random overlap assumption occur over the vast ocean, particularly poleward of 40°C , the study therefore suggest that a linear combination of minimum and random overlap assumptions may further improve the predictions of actual cloud fractions for multilayered cloud types (e.g., As+St/Sc and Ac+St/Sc) over the Southern Ocean. The establishment of statistical relationship between multilayered cloud types and the environmental conditions (e.g., atmospheric vertical motion, convective stability and wind shear) would be useful for parameterization design of cloud overlap in

numerical models.

1. Introduction

As the most important regulators of the Earth's climate system, clouds significantly affect the radiation budget, the hydrological cycle and the large-scale circulation of the Earth (Hartmann et al., 1992; Stephens, 2005). However, because of incomplete knowledge of their underlying physical processes, clouds are still poorly represented in climate and weather models (Zhang et al., 2005) and are considered a major source of uncertainty in climate change predictions by GCMs (Cess et al., 1990).

Cloud types, which represent important cloud macro-physical properties, are particularly significant in the Earth's radiation budget and hydrological cycle. Cloud types are governed by different types of atmospheric motion and are associated with different microphysical properties; thus, distinct cloud radiative effects and precipitation occur for each cloud type (Ackerman et al., 1988; Betts and Boers, 1990; Hartmann et al., 1992). However, multilayered cloud systems, in which two or more cloud types are simultaneously present over the same location but at different levels in the atmosphere, have been frequently reported by surface and aircraft observations (Tian and Curry, 1989). The frequent co-occurrences of different cloud types in the atmosphere increase the complexity of present cloud climatology studies. For example, the effects of individual cloud types on the surface and atmospheric radiation budgets depend on whether other clouds are also present above or below them. In addition, cloud overlap variations can significantly change atmospheric radiative heating/cooling rates, atmospheric temperatures, hydrological processes, and daily variability (Chen and Cotton, 1987; Morcrette and Jakob, 2000; Liang and Wu, 2005). Therefore, to improve radiation calculations of climate prediction models, understand cloud physical processes, and evaluate the schemes for generating clouds in those models, it is necessary to know the amount and distribution of each cloud type, particularly a detailed description of the co-occurrence of different cloud types

and their statistical properties.

Until recently, many related studies on cloud types and cloud overlap, which are based on several fundamentally different types of passive observational datasets (typically the International Satellite Cloud Climatology Project (ISCCP) and surface observer reports), have focused on the geographical distributions and long-term variations of cloud types (e.g., Rossow and Schiffer, 1991; Rossow and Schiffer, 1999; Hahn et al., 2001; Warren et al., 2007; Eastman et al., 2011; Eastman et al., 2013), cloud radiative effects (Hartmann et al., 1992; Chen et al., 2000; Yu et al., 2004), cloud-property retrievals in multilayered clouds using multi-channel measurements from passive sensors (Chang and Li, 2005a, Chang and Li, 2005b; Huang et al., 2005; Huang et al., 2006a; Huang et al., 2006b; Minnis et al., 2007), and the statistics of cloud overlap based on surface weather reports and measurements from ground-based cloud radar (Warren et al., 1985; Hogan and Illingworth, 2000; Minnis et al., 2005). However, these studies have limitations and uncertainties because passive detection methods and cloud-classification algorithms generally fail to detect multilayered clouds effectively. First, the existence of overlapping cloud layers may obscure the upper-level clouds from the perspective of a ground-based weather reporter, and lower clouds may be hidden from the view of a passive satellite. As a result, surface observer reports and ISCCP significantly underestimate high and low cloud frequencies and introduce significant biases into the trend analysis of cloud cover, retrievals of cloud properties and evaluations of cloud radiative effects. Second, most of these studies are limited to specific locations and time periods or multilayered cloud systems. Systematic studies on the statistical co-occurrence of different cloud types on a global scale have received far less attention.

Fortunately, the millimeter-wavelength cloud-profiling radar (CPR) on CloudSat (Stephens et al., 2002) and the cloud-aerosol lidar with orthogonal polarization (CALIOP) (Winker et al., 2007) on CALIPSO (launched in late April 2006) provide an unprecedented opportunity for detailed studies on the three-dimensional structures of clouds on a global scale. Since mid-June 2006, CALIPSO and CloudSat data have been widely used to investigate the three-dimensional distributions and structures of

hydrometeors and to improve the cloud-overlap assumption used in GCMs (e.g., Barker, 2008; Luo et al., 2009; Kato et al., 2010; Li et al., 2011). By using a radar-only cloud-classification product (i.e., the 2B-CLDCLASS dataset from CloudSat), Sassen and Wang (2008) presented the geographical distributions and global average frequency of each cloud type. In this study, we investigate the co-occurrence frequencies of different cloud types and analyze their along-track horizontal scales and radiative effects using the latest cloud-classification and radiative-flux products based on the combined measurements of the two active sensors mentioned previously. Finally, we perform a preliminary evaluation of how well cloud-overlap assumptions characterize the overlap of two apparently separate cloud types. Although some statistical results reasonably agree with previous studies, new insights are achieved in this investigation. These new results will hopefully be useful for future GCMs evaluations and improvements.

The study is organized as follows. The dataset for the research is described in Section 2. Section 3 provides the zonal distributions and global statistics of the co-occurrence frequencies of cloud types and discusses their along-track horizontal scales and radiative effects. An evaluation of the performance of cloud-overlap assumptions based on the co-occurrence frequencies of cloud types is presented in Section 4.

2. Data

In the following study, four years (2007-2010) of data from the latest release of the CloudSat 2B-CLDCLASS-Lidar (version 1.0) product (i.e., Radar-Lidar cloud classification) and the 2B-FLXHR-LIDAR product are collected to analyze cloud types and discuss their co-occurrence frequencies, horizontal scales and radiative effects.

The ISCCP uses a combination of cloud-top pressure and cloud optical depth to classify clouds into cumulus, stratocumulus, stratus, altocumulus, altostratus, nimbostratus, cirrus/cirrostratus, and deep convective clouds. However, traditional surface observations identify clouds by using basic features (e.g., base height, horizontal and vertical dimensions, and precipitation types) of the major cloud types

(World Meteorological Organization, 1956; Parker, 1988; Moran et al., 1997). Based on these basic cloud characteristics, Wang and Sassen (2001) classified cloud types into eight classes by combining the range capabilities of active sensors (radar and lidar) and the auxiliary measurements from the other passive sensors (e.g., infrared and microwave radiometers); they further indicated the overall agreement (approximately 70%) between the results from their algorithm and the surface visual observations from the Southern Great Plains (SGP) CART site.

Based on the algorithm presented by Wang and Sassen (2001), the Radar-Lidar cloud classification identifies the cloud types using two steps. First, combined radar and lidar cloud-mask results are used to find a cloud cluster according to cloud persistence in the horizontal and vertical directions. By performing the cloud clustering analysis, a CloudSat granule may be divided into a number of cloud clusters, depending on the cloud systems present. Once a cloud cluster is found, the cloud height and phase, maximum effective radar reflectivity factor (Z_e) and temperature, and the occurrence of precipitation are determined. Second, the cluster mean properties and spatial inhomogeneities, in terms of the cloud-top heights and maximum signals of the radar and lidar, are sent to a fuzzy classifier to classify the cluster into one cloud type with an assigned confidence level. To improve the classification flexibility, a combination of rule-based and fuzzy-logic-based classification is used in this algorithm. The cloud-phase determination is based on rules, and the cloud-type classification is mainly based on fuzzy logic (see Wang et al., Level 2 Combined Radar and Lidar Cloud Scenario Classification Product Process Description and Interface Control Document, version 1.0, 2013, available at <http://www.cloudsat.cira.colostate.edu/dataICDlist.php?go=list&path=/2B-CLDCLSS-LIDAR>). The cloud types provided by this product (version 1.0) include high clouds (High), altostratus (As), altocumulus (Ac), stratus (St), stratocumulus (Sc), cumulus (Cu), nimbostratus (Ns) and deep convective (Dc) clouds. The High cloud type includes cirrus, cirrocumulus and cirrostratus, and the Cu cloud type represents cumulus congestus and fair weather cumulus. Following the study of Sassen and Wang (2008), we also combine two cloud types (St and Sc) into St+Sc in the present

study. By combining the unique complementary capabilities of the cloud profile radar (CPR) of CloudSat and the space-based polarization lidar (CALIOP), some CPR weaknesses (e.g., high surface contamination in the lowest three to four vertical bins of the CPR and a lower sensitivity to optically thin clouds) are minimized in the latest Radar-Lidar cloud classification product; thus, the identification of High (cirrus or cirrostratus) and low cloud types (such as St, Sc and Cu) is significantly improved in the 2B-CLDCLASS-Lidar product.

By using CloudSat microphysical retrievals, a combined CloudSat/CALIPSO cloud mask and lidar-based aerosol retrievals as inputs for a broadband, two-stream, plane-parallel, adding-and-doubling radiative transfer model, the 2B-FLXHR-LIDAR product provides calculated radiative fluxes and atmospheric heating rates at 240 m vertical increments (Henderson et al., 2013). Incorporating the radiative influence of optically thin and low clouds that were undetected by CloudSat significantly improved the agreement between the 2B-FLXHR-LIDAR calculations and observations from the Clouds and the Earth's Radiant Energy System (CERES) experiment. Henderson et al. (2013) showed that the global mean outgoing shortwave radiation (OSR) and outgoing longwave radiation (OLR) estimated from the collocated CERES observations and 2B-FLXHR-LIDAR calculations agree within 4 and 5 W/m², respectively, with root-mean-square differences of 6 W/m² and 16 W/m² on monthly/5° scales. Because the passive sensors largely fail to resolve the cloud overlap in the vertical, the 2B-FLXHR-LIDAR product derived from these two active sensors is considered a vital dataset for examining the radiative heating features in the atmosphere and for studying the variations in fluxes and heating rate caused by vertically overlapping clouds (L'Ecuyer et al., 2008; Haynes et al., 2013). In this investigation, we focus on the radiative effects of different multilayered cloud types at the TOA and at the surface during the daytime by using the 2B-FLXHR-LIDAR.

The following cloud parameters in the 2B-CLDCLASS-Lidar product are used in this study: cloud layer (CL) and cloud layer type (CLTY). In the 2B-FLXHR-LIDAR product, only the TOACRE (cloud radiative effect at the TOA) and BOACRE (cloud radiative effect at the surface) are used. Here, we consider one data profile as a

multilayered (or single-layered) cloud profile when two or more cloud layers (or only one layer) are present within the vertical profile based on the parameter “cloud layer”. To map the regional variability in the studied variable, we group the global area into $2^{\circ} \times 2^{\circ}$ grid boxes to collect a sufficient number of samples in each grid box. Following the definitions of cloud fraction and cloud amount proposed by Hagihara et al. (2010), the cloud-type fractions and amounts in a given grid box are defined as the number of particular cloud-type profiles divided by the number of total sample profiles and the total cloud profiles within this box, respectively. For example, the cloud fraction for multilayered clouds is the ratio of the number of multilayered cloud profiles to the number of total sample profiles in a given grid box. In this investigation, we only provide the annual average cloud properties of different overlapping cloud types with small seasonal variations. In addition, comparisons of the four-year average cloud fractions for different cloud types between daytime and night-time are provided in tables. Notably, the day-night comparisons of cloud fractions are only represented by the two overpass times of the satellites. The full diurnal cycle cannot be captured by CALIPSO and CloudSat. Sassen et al. (2009) showed that the observed day-night variations in cirrus observed by CALIPSO mostly reflect real cloud processes, even when the strong solar noise signature impacts the comparisons of cloud types between day and night, particularly for cirrus. For other cloud types, the uncertainty caused by the daylight noise for lidar may be smaller. Thus, the calculated annual mean cloud fractions for different cloud types in this investigation are reliable.

3. Simultaneous co-occurrence of different cloud types

3.1. Zonal distributions of overlapping clouds

Multilayered cloud systems frequently occur in the atmosphere. Our statistical results show that the seasonal variations in multilayered cloud percentages are small, and the seasonal globally averaged values range between 25% and 28%. These results are comparable to the multilayered cloud fractions (approximately 27%) from the Geoscience Laser Altimeter System (GLAS) (Wylie et al., 2007). Furthermore, we plot the global and zonal distributions of the annually averaged multilayered cloud

fractions (see Fig.1). In Fig.1a, the high-value and low-value centers of the multilayered cloud fractions are very obvious. For example, equatorial central South America, western Africa, Indonesia and the west-central Pacific Ocean warm pool are typical high-value centers. There are three obvious peaks in the zonal mean patterns (Fig.1b): one major peak occurs in the tropics, and two minor peaks occur in the midlatitudes; two local minima occur in the subtropics. The local maximum during spring (thick, black line) in the northern midlatitudes may be the result of misidentifying high-level dust transport as high ice clouds or the result of the actual influences of dust on ice nucleation (Chen et al., 2010; Yu et al., 2012; Yuan and Oreopoulos, 2013).

In all multilayered clouds, we further identify the most frequently multilayered cloud systems (annually) and provide their zonal distributions (Fig. 2). Note that the overlap of the same cloud type (e.g., High+High) is not important in numerical climate simulations because these clouds have similar cloud properties and temperatures. Thus, treating these clouds as a single layer may not introduce serious errors into the calculation of the cloud properties (Wang and Dessler, 2006). In addition, the overlap of specific two cloud types in any three or more layer cloud systems (e.g., High+As+Cu) is also included in statistical results of their occurrence frequencies. But, only two layer cloud systems is used when we calculate the weighted cloud radiative effect of specific two cloud types-overlap in section 3.3. Fig. 2 clearly indicates that the zonal patterns of different combinations of cloud types are very different. For example, multilayered cloud systems that include high clouds either have one peak in the tropics (High+Ac and High+Cu) or three peaks in the tropics and midlatitudes (High+St/Sc, High+Ns and High+As). The high clouds that represent the major peak in the tropics may be caused by large-scale ascent or by dissipating deep convection. However, gentle large-scale ascent and ice cloud production within frontal convection are likely responsible for the two minor peaks of the multilayered cloud systems along midlatitude storm tracks. In addition to these combinations of cloud types, As-over-stratiform clouds or Ac-over-stratiform clouds also tend to be concentrated in the midlatitudes (60° and poleward). In fact, the

distributions of clouds in different geographical regimes may depend on environmental factors in these regimes, such as sea surface temperature, lower tropospheric stability, and vertical velocity (Klein and Hartmann, 1993; Norris and Leovy, 1994). By studying the relations between various cloud types and the sea surface temperature of the tropical oceans, Behrangi et al. (2012) indicated that as the SST increases, the fraction of multilayered clouds increases up to a SST of 303 K and then decreases for SSTs greater than 303 K. The ranges of SSTs are very different for different combinations of cloud types, e.g., high clouds over St/Sc or Ns clouds tend to occur between 292 and 294 K, but high clouds over Ac, As or Cu clouds tend to occur between 302 and 304 K, even though almost all of the clouds have major peak values in the tropics. In addition, Yuan and Oreopoulos (2013) indicated that the vertical velocity of large-scale pressure systems has a negative correlation with the percentage of multilayered cloud systems. Strong subsidence favors low cloud formation and suppresses ice cloud generation; thus, multilayered clouds are infrequent over major Sc-dominated oceanic areas at latitudes near 30°.

However, multilayered cloud systems are very difficult to detect by passive satellites (such as ISCCP) and by surface weather reporters, particularly during the night-time and for cloud systems that include very thin cirrus (Sassen and Cho, 1992; Liao et al., 1995). For example, when a high-level transparent cirrus cloud overlies a boundary layer stratus cloud, the retrieved cloud-top heights typically lie between the cirrus and stratus cloud heights (e.g., Baum and Wielicki, 1994), leading to the misinterpretation of cloud types by ISCCP. For cloud property retrievals, the influence of liquid water clouds and precipitation on the radiances observed at the TOA is also one of the greatest impediments to determining the cloud ice mass for multi-layered systems that include ice clouds above water clouds (Huang et al., 2006a).

3.2. Global statistics of cloud overlap

The global average percentage overlap of different combinations of cloud types over land or ocean during the daytime and night-time are provided in Tables 1 and 2, respectively. These tables show that high clouds, As, Ac and Cu are much more likely

to co-exist with other cloud types, regardless of the time of day or surface type. The frequency of High-over-Ac may even exceed the frequency of single-layered Ac clouds, indicating that these two types actually exhibit a stronger meteorological association. However, under large-scale subsidence regions, St/Sc and Ns are much more likely to exhibit individual features, particularly St/Sc over the ocean. Convective clouds are also typically in single layers. Although Cu form in unstable air and As form in stable air, a small percentage of overlap occurs. Globally, 44% (50%) and 35% (39%) of low clouds (St/Sc +Cu) over land and ocean during the daytime (night-time) are overlapped by other cloud types aloft. Approximately 23% (26%) and 20% (25%) of low clouds over land and ocean during the daytime (night-time) are connected with high clouds. These percentages are comparable to those (approximately 30%) presented by Yuan and Oreopoulos (2013). Notably, high clouds also include cirrostratus and cirrocumulus; thus, the percentage of overlap of deep convection below high clouds is approximately 29%, which is larger than the percentage (approximately 24%) of cirrus-over-convection clouds based on ICESat/GLAS (Geoscience Laser Altimeter System) (Wang and Dessler, 2006).

Based on the above figures and tables, we plot the global distributions of the annual mean dominant cloud types and their cloud fractions. Here, the cloud types include all single-layered and multilayered cloud systems (see Fig. 3a-3b). Fig. 3c-3d shows that the global distributions of the annual mean cloud types (only for multiple dominant clouds) and corresponding cloud amounts. Based on Fig.3a-3b, St/Sc is the dominant cloud type worldwide, particularly over the ocean. High clouds are mainly concentrated in the tropics and subtropics. In addition, over Antarctica, the most frequent cloud type is As. These results are in reasonable agreement with the findings based on the ISCCP D1 dataset (Doutriaux-Boucher and Seze, 1998). However, Fig. 3a-3b also shows that As prevails over the arid/semi-arid land in the Northern Hemisphere, such as northwestern China and North America. In contrast, Ac is dominant over the arid/semi-arid land of the Southern Hemisphere, such as Australia and southern Africa. However, not all of these features are observed by Doutriaux-Boucher and Seze (1998) using the ISCCP D1 dataset. In fact, the obvious

regional and seasonal variations in Ac and As are possibly related to the frequency of dust activities (Choi et al., 2009). In addition, over some deserts (such as the Sahara Desert), the most prevalent cloud type is low-level clouds (St/Sc) according to the ISCCP D1, as opposed to the high clouds in our results. This discrepancy may be due to inadequate identification of airborne dust, such as the ISCCP misclassifying dust as low-level clouds, as suggested by the low values of the effective droplet radius reported by Han et al. (1994) over these regions.

Generally, the High-over-St/Sc and High-over-Cu cloud systems are more common over the vast oceans of the tropics and midlatitudes, while High-over-Ac cloud systems tend to exist over land at the same latitudes (see Fig. 3c). Notably, As-over-Cu only occurs over northwestern China. In addition, the As-over-St/Sc cloud systems are dominant in the high latitudes. Fig. 3d shows the multilayered cloud-type amount, defined as the ratio of the cloud fraction of one multilayered cloud combination to the cloud fraction of total multilayered cloud systems. In addition, we note that some multilayered cloud systems (High-over-St/Sc) exist over the major Sc-dominated oceanic areas, which are generally unfavorable for upper-level cloud formation due to persistent strong subsidence. The major source of high clouds is topography-driven gravity wave activity, advection from neighboring tropical convection centers, such as the Amazon Basin or the Congo Basin, or ascent associated with midlatitude fronts.

3.3. Along-track horizontal scales and radiative effects of cloud overlap

The horizontal scale of a multilayered cloud system along the CALIPSO/CloudSat track is determined by calculating the number of continuous profiles (N), in which each profile includes a vertical column with a particular combination of cloud types. Considering the 1.1 km along-track resolution of CPR measurements, the along-track scale (L in km) of a multilayered cloud system is $L = N \times 1.1$ (Zhang et al., 2014).

Fig. 4a-4d presents the zonal variation in the along-track horizontal scales of clouds in the multilayered cloud systems and their probability distribution functions (PDFs). As shown in Fig. 4a-4b, the High+St/Sc, As+St/Sc, High+Ns and High+Dc cloud systems have obvious zonal variations. High+St/Sc and As+St/Sc have

minimum scales (approximately 10 km) in the tropics and maximum scales (up to 20 km) poleward of 40° (i.e., along the storm tracks). However, the along-track horizontal scales of High+Ns and High+Dc decrease from the tropics to the poles. The zonal variations in the scales of other clouds systems are small, particularly for High+Cu, As+Cu and Ac+Cu (approximately 3 km). We also provide the global average along-track horizontal scales and standard deviation (STD) of these cloud systems in Fig. 4c-4d. Generally, As+St/Sc has a maximum scale (17.4 km) and STD (23.5 km), while Ac+Cu has a minimum scale (2.8 km) and STD (3.1 km). Based on the relatively larger scales of STDs than mean values, it is clear that the along-track horizontal scales of these cloud systems all have larger variations globally. By assuming a typical grid resolution of 1° in global climate models, we find that all multilayered cloud types cannot be resolved by global climate models. The multilayered cloud systems that include Cu (such as High+Cu, Ac+Cu and As+Cu) are not even captured by regional climate models with higher grid resolutions (approximately 15 km).

Furthermore, Fig. 5a-5b shows the zonal distributions of the TOA cloud radiative effects of these multilayered cloud systems during the daytime. In addition, we also provide the zonal distributions of weighted cloud radiative effects by considering the frequency of occurrence of each cloud type during the daytime only (Fig. 5c-5d). Although the zonal distributions of the cloud radiative effects for these cloud systems are similar, i.e., decrease from the tropics to high latitudes, the radiative effects can be grouped into several distinct classes. For example, middle-over-low (such as As+Sc/St and As+Cu) cloud systems have comparable radiative effects (maximum value of -300 W/m²), while high-over-low (such as High+Sc/St and High+Cu) cloud systems have small radiative effects (maximum value of -150 W/m²). By considering the weight of each multilayered cloud type, we find that the contributions to the cloud radiative effect of the whole multilayered cloud system are different (Fig. 5c-5d). In the tropics, High+Ac and High+Cu contribute -9 W/m² and -8 W/m², respectively, to the cloud radiative effects. Other cloud types have obvious zonal distributions, and their contributions range from 0 to -6 W/m². In mid-high latitudes, some

mid-over-low (such as As+Sc/St) cloud systems are more important to the regional energy balance, particularly over the Southern Ocean regions. Similar to Fig. 5, Fig. 6 presents the surface-based results during the daytime. In summary, the trends are similar, but all cloud types have larger radiative effects at the surface than at the TOA; specifically, the effect is an obvious surface cooling. Clearly, the energy differences in the cloud radiative effects between the surface and the TOA are persistent and may significantly change the atmospheric radiative heating/cooling rates and temperature; however, the impacts are very different for the multilayered cloud types. The cloud types all cause weak atmospheric heating (of approximately $0.5\text{--}3\text{ W/m}^2$) at low latitudes and midlatitudes, whereas weaker atmospheric cooling can be observed at high latitudes for some multilayered cloud types (e.g., As+Sc/St, Ac+Sc/St and High+Sc/St).

On a global scale, the range of the global mean radiative effect of the cloud systems is -100 W/m^2 to -350 W/m^2 , except for High+Dc (the black dots are the mean values and the lines represent the standard deviation in Fig. 7a-7b). In Fig. 7c-7d, the black bars represent the weighted radiative effects of each cloud type at the TOA and surface. Generally, the global mean cloud radiative effects are approximately -103.1 W/m^2 and -118.8 W/m^2 at the TOA and at the surface, respectively. The percentages of radiative contributions from multilayered cloud systems are 40.1% (approximately -41.3 W/m^2) and 42.3% (approximately -50.2 W/m^2) at the TOA and at the surface, respectively. Clearly, the existence of a multilayered cloud system is important to Earth's radiative energy balance. A further analysis shows that two-layered and three-layered (or more layers) cloud systems contribute approximately -27.2 W/m^2 (-33.1 W/m^2) and -14.1 W/m^2 (-17.1 W/m^2), respectively, to the total cloud radiative effect at the TOA (surface). However, the radiative effects of ten multilayered cloud types are -22.7 W/m^2 and -27.1 W/m^2 at the TOA and at the surface (a contribution of 22%). High+Ac and High+Sc/St (or Cu) have relatively smaller effects than High+Dc and Ac+Sc/St (or Cu), but their contributions to the cloud radiative effect of the whole multilayered cloud system are highest because of their more frequent occurrence, larger weights (see the gray line in Fig. 7c-7d), and distribution from the tropics to the

midlatitudes (Fig. 3). However, the other cloud types may be important to regional cloud radiative effects. For example, mid-to-upper level clouds frequently coexist with boundary layer clouds (e.g., As+St/Sc and High+St/Sc) over the Southern Ocean; thus, mid-atmosphere cloudiness is overestimated by ISCCP and is partially responsible for the TOA shortwave radiation bias in the climate models over this region (Haynes et al., 2011).

4. Evaluation of cloud-overlap assumptions based on cloud types

Based on the advantages of the two active sensors, we preliminarily evaluate how well the cloud-overlap assumptions can characterize the overlap of two apparently separate cloud types using the 2B-CLDCLASS-Lidar cloud type product. The cloud overlap assumption has been widely used to describe the actual vertical distribution of clouds and the parameterization of the total cloud fraction in a given model grid box. Several basic cloud-overlap assumptions have been proposed, such as maximum, random, random-maximum and minimum overlaps (Hogan and Illingworth, 2000). The most common cloud-overlap scheme in current GCMs is called “random-maximum” overlap, which assumes that cloud layers separated by clear layers are randomly overlapped, while vertically continuous cloud layers have maximum overlap (Stephens et al., 2004). When the cloud fractions of the upper and lower layers are C_1 and C_2 , the total cloud fractions of the two cloud layers based on the overlap assumptions are given by:

$$\begin{aligned} C_{random} &= C_1 + C_2 - C_1 \times C_2, \\ C_{max} &= \max(C_1, C_2), \text{ and} \\ C_{min} &= \min(1, C_1 + C_2). \end{aligned} \tag{1}$$

In addition, if we know the actual overlap fraction $C_{overlap}$, then the observed total cloud fraction C_{real} can be written as:

$$C_{real} = C_1 + C_2 - C_{overlap} \tag{2}$$

However, Hogan and Illingworth (2000) proposed a simpler and more useful expression for the degree of cloud-layer overlap (exponential random overlap). In the expression, the mean observed cloud fraction of two cloud layers can be determined by the linear combination of the maximum and random overlap in terms of an

“overlap parameter” a ,

$$C_{real}=a \times C_{max}+(1-a) \times C_{random} \quad (3)$$

Here, the overlap parameter a is considered a function of the layer separation, and related to the vertical resolution and the horizontal domain size. $a=0$ is random overlap and $a=1$ is the maximum overlap. As C_{real} increasingly departs from C_{max} (trending toward C_{min}), a becomes negative, indicating a tendency for an even lower degree of overlap than that predicted by the random overlap assumption. Besides vertical resolution and the horizontal domain size, the degree of cloud overlap also depends on the dynamics and atmospheric state (such as, atmospheric vertical motion, convective stability and wind shear) (Naud et al., 2008). For example, vertically continuous clouds to be more maximally overlapped in the presence of vertical motion in midlatitudes and decreased convective stability in the Tropics. However, large wind shears were found to increase the randomness of the overlap, with overlap becoming less than random in some cases ($a<0$). Based on several months of data from ICESat/GLAS observations, Wang and Dessler (2006) showed that overlap differences between the observed and random overlaps exist when describing the actual overlap of two separated cloud types (vertical separation >0.5 km). However, the authors’ work focused on the tropics and was limited to simple cloud classifications using space-based lidar. We expand the study by Wang and Dessler (2006) by employing a global-scale analysis and a more complete cloud classification; the overlap of two separate cloud types in each combination of cloud types in each grid box is determined. Moreover, we evaluate the performances of the random overlap assumption and calculate the overlap parameter a for each multilayered cloud type in each grid box.

We first group each multilayered cloud system. For example, for the High+St/Sc multilayered cloud systems in the same grid box, we consider two layers and group all high clouds into the upper layer and all stratiform clouds into the lower layer, rather than conveniently grouping the clouds into multiple layers according to the vertical separation of two types. Then, four possible values for the combined cloud fraction of the two cloud types at different layers are calculated by assuming random overlap,

maximum overlap, minimum overlap and actually observed overlap. Because random cloud overlap is considered a better characterization of cloud overlap behavior than minimum overlap and maximum overlap, we only provide the difference in the cloud fractions between random overlap and actually observed overlap. Finally, the overlap parameter a for each multilayer in each grid is calculated based on Eq. (3). Notably, because we do not group multilayered cloud types into multiple layers according to the vertical separation of two types, only one value for the overlap parameter a for each multilayered cloud system in each grid is obtained. a may be considered the mean value of all overlap parameters at different layer separations. Here, we define the relative difference (RD) between the random and actual overlap for one of the multilayered cloud types as:

$$RD = (C_{random} - C_{real}) / C_{real} \quad (4)$$

In addition, the cumulative relative difference (CRD) between the random and actual overlap for all multilayered cloud types (approximately 17 different combinations of different cloud types) in each $2^\circ \times 2^\circ$ grid box is given by:

$$CRD = \sum_{i=1}^{17} RD^i \times w^i \quad i=1, 2, 3 \dots, 17 \quad (5)$$

Similar to the definition of CRD, we define the cumulative overlap parameter (COP) in each $2^\circ \times 2^\circ$ grid box as:

$$COP = \sum_{i=1}^{17} a^i \times w^i \quad i=1, 2, 3 \dots, 17 \quad (6)$$

where w is the weight coefficient for one multilayered cloud type in each $2^\circ \times 2^\circ$ grid box as follows:

$$w^i = f^i / \sum_{i=1}^{17} f^i \quad i=1, 2, 3 \dots, 17 \quad (7)$$

f is the cloud fraction of each multilayered cloud type in every grid box.

Fig. 8a-8b shows the zonal distributions of the relative differences for ten of the main multilayered cloud types and the cumulative relative differences for all multilayered cloud types (gray line). The results show that differences exist, even though the random-cloud-overlap assumption is thought to better describe cloud-overlap behavior than other schemes when the cloud layers appear to be separate. The cloud fractions based on the random-overlap assumption are underestimated for High+St/Sc,

As+St/Sc and Ac+St/Sc at all latitudes; these differences can exceed -5%. The cloud
 fraction of the High-over-Ac system is overestimated at all latitudes. The peak values
 of the difference are mainly located in mid- and high- latitudes in both hemispheres
 and are up to 5%. For other types, the relative differences are smaller and change with
 latitude. In summary, the cumulative relative difference of all multilayered cloud
 types is small (gray lines), and almost values are negative at all latitudes. In Fig. 8c-8d,
 we further show the zonal distributions of the overlap parameter for ten of the main
 multilayered cloud types and the cumulative overlap parameter of all multilayered
 cloud types. Clearly, the overlap parameters for High+St/Sc, As+St/Sc and Ac+St/Sc
 at all latitudes are negative, indicating a C_{real} departure from C_{max} (trending toward
 C_{min}) and a tendency for an even lower degree of overlap than predicted by the
 random overlap assumption. Thus, the linear combination of maximum and random
 overlap assumptions is problematic due to the negative overlap parameters in those
 regions, where the three multilayered cloud types mentioned above are dominant,
 particularly over the major Sc-dominated oceanic areas. However, the overlap
 parameters are positive for High+Ns and High+Ac. Thus, C_{real} has a value between
 C_{max} and C_{random} , and the exponential random overlap can predict the actual overlap of
 these two types very well. These results are intuitive, as cloud types are governed by
 different types of atmospheric motion and state. The formation of cumuli-form clouds
 may be related to the strong ascent or convectively unstable which result in clouds
 that increase in height more quickly, and increasing the degree of overlap with other
 cloud types. However, random or minimum overlap occurs preferentially in regions of
 subsidence or convective stability (favors strati-form cloud). Therefore, it is not
 difficult to understand why the zonal distributions of cloud overlap parameters are
 very different for similar cloud overlap systems (e.g., middle-over-low). For example,
 the overlap parameters of As+St/Sc and Ac+St/Sc over the Southern Ocean are
 obviously distinct from As+Cu and Ac+Cu. In summary, the cumulative overlap
 parameters of all multilayered cloud types (gray lines) are negative at nearly all
 latitudes. However, two points still require further interpretation. First, the cumulative
 overlap parameters in the tropics and in the Northern Hemisphere have small values

(and possibly positive values); thus, random overlap or exponential random overlap is representative of the actual conditions. Second, in the Southern Hemisphere, the cumulative overlap parameters trend toward C_{min} ; thus, a better prediction using random overlap or exponential random overlap is difficult. This finding partially explains why the climate model errors in the TOA fluxes over the Southern Ocean are the largest (Trenberth and Fasullo, 2010). Based on the global results from this study, we also further support the findings of Naud et al. (2008) that factors such as dynamics could be connected to the way cloudy layers overlap. As a result, we suggest that a linear combination of minimum and random overlap assumptions may further improve the predictions of real cloud fractions for the multilayered cloud types in the Southern Hemisphere (e.g., As+St/Sc and Ac+St/Sc), particularly poleward of 40 °S over the ocean. However, only three cloud types (e.g., low-level marine stratus, convective cloud and layered cloud) are diagnosed by the cloud scheme in current GCMs. To be useful for parameterization design, it is necessary for the overlap behavior we observe to be related to quantities predicted by a GCM. In view of the cloud types are governed by different types of atmospheric motion and state, we thus consider environmental conditions related to cloud formation as a means to parameterize the overlap characteristics in numerical models. But, before that, statistical connection between multilayered cloud types and the environmental conditions should be established in the future studies by using global cloud-overlap and meteorological reanalysis datasets.

The global distributions and statistical results of the cumulative relative difference and the cumulative overlap parameter for all multilayered cloud types are shown in Fig. 9 and Tables 3 and 4, respectively. Fig. 9a shows the cumulative relative difference, whereas Fig. 9b shows the cumulative overlap parameter. In Fig. 9a, we find that the cloud fractions based on the random overlap assumption are underestimated over the vast ocean, except over the west-central Pacific Ocean warm pool. Obvious overestimations occur over tropical and subtropical land masses, particularly where low multilayered cloud fractions are found, such as in equatorial central South America, southern and northern Africa, Australia and the Antarctic. In

these regions, the High-over-Ac system is the dominant multilayered cloud type. This pattern indicates that land surface effects may favor an exponential random overlap. In Fig. 9b, the distributions of the cumulative overlap parameter are similar to the results of the cumulative relative difference. Negative overlap parameters also occur over the vast ocean, except over the west-central Pacific Ocean warm pool. The typical negative high-value centers correspond to the major Sc-dominated oceanic areas very well. The positive overlap parameters are mostly located over tropical and subtropical land masses and Antarctica. Globally, by using random overlap, the overlap percentages are overestimated by 24%, 21.9%, 30% and 133.3% for High clouds over As, St/Sc clouds, Ns, and Ac over St/Sc clouds, respectively, over land during the daytime (Table 3). An overestimation also occurs for As over Cu and St/Sc clouds. However, the overlap of High clouds with Ac and Cu is underestimated by -32.6% and -25% over land during the daytime, respectively. Regardless of vertical separation of two types, the absolute errors of cloud-type fractions (See Tables 3 and 4) seem small for global mean, but we should recall the previous finding that a 4% increase in low cloud cover would be sufficient to offset the warming effect of a doubling of CO₂ (Randall et al. 1984), therefore, these bias errors in cloud cover possible induce a substantial bias error in the regional radiation budget. The underestimations (or overestimations) of the cloud fraction by the random overlap assumption ultimately cause overestimations (or underestimations) of cloud radiative effects. Globally, the overestimations of the cloud radiative effect are obvious for High+St/Sc and Ac+St/Sc (approximately 3.9 W/m² at the surface, about 3.3% of the mean cloud forcing), whereas the underestimations of the cloud radiative effect are obvious for High+Ac and High+Cu (Table 3). Generally speaking, change in cloud forcing caused by these bias errors in cloud cover is about 11 W/m² at the surface, about 10% of the mean cloud radiative effect at the surface. Thus, if these bias errors in cloud cover codified in GCMs, could bias climate feedbacks resulting from increasing trace gasses or natural variability.

5. Summary and discussion

Although cloud types and their co-occurrence variations are the most significant

components of the global climate system and cloud climatology studies, systematic and global studies on statistical properties of clouds have not received much attention. This study quantitatively evaluates the co-occurrence frequencies of different cloud types, analyzes their along-track horizontal scales and radiative effects by using the latest cloud classification (2B-CLDCLASS-Lidar) and radiative flux products (2B-FLXHR-LIDAR) based on 4 years of combined measurements from CALIPSO and CloudSat. We also preliminary evaluate cloud-overlap assumptions. Although some statistical results reasonably agree with previous research, new insights are also achieved in this paper.

The statistical results clearly show that High clouds, As, Ac and Cu are much more likely to co-exist with other cloud types. However, St/Sc and Ns, which are typically under large-scale subsidence regions, and convective clouds are much more likely to exhibit individual features. The zonal variations in along-track horizontal scales are distinct for different multilayered cloud systems. On average over the globe, As+St/Sc has a maximum scale (17.4 km) and STD (23.5 km), while Ac+Cu has a minimum scale (2.8 km) and STD (3.1 km). Generally, the percentages of radiative contributions from multilayered cloud systems are 40.1% (-41.3 W/m²) and 42.3% (-50.2 W/m²) at the TOA and at the surface, respectively. However, the radiative effects of ten multilayered cloud types are -22.7 W/m² and -27.1 W/m² (a radiative contribution of 22%) at the TOA and at the surface, respectively, during the daytime. High+Ac and High+Sc/St (or Cu) cloud systems dominate the weighted global mean cloud radiative effects because they are most frequent.

Active sensors allow us to preliminarily evaluate how well the overlap assumptions describe the actual overlap of two separate cloud types. In summary, the cloud fractions based on the random overlap assumption are mainly underestimated over the vast ocean, except over the west-central Pacific Ocean warm pool. Obvious overestimations occur over tropical and subtropical land masses, particularly in regions with low multilayered cloud fractions. These bias errors in cloud cover may induce a substantial bias error in the regional radiation budget. Globally, change in cloud forcing caused by these bias errors is about 11 W/m² at the surface, contributes

an about 10% of the mean cloud radiative effect at the surface. Considering that negative overlap parameters occur over the vast ocean, particularly poleward of 40 °C, we suggest that a linear combination of minimum and random overlap assumptions may further improve the predictions of actual cloud fractions for multilayered cloud types (e.g., As+St/Sc and Ac+St/Sc) over the Southern Ocean. Obvious zonal variations of overlap parameters for different multilayered cloud systems also verify that factors such as dynamics related to cloud formation could be connected to the way cloudy layers overlap. Therefore, we may consider environmental conditions as a means to parameterize the overlap characteristics in order to be useful for parameterization design in numerical models. In addition, the seasonal variations of cloud overlap also must be studied, as one would expect if cloud systems are driven by processes related to convection during the warm season and synoptic scale systems during winter (Mace et al., 2002).

Previous studies have quantitatively evaluated the global mean cloud fraction of each cloud type using various datasets (such as ISCCP). However, we identify new features that were not observed with the ISCCP D1 dataset (Doutriaux-Boucher and Seze, 1998). For example, As and Ac prevail over the arid/semi-arid land of the Northern Hemisphere (northwestern China and North America) and Southern Hemisphere (Australia and southern Africa), respectively. Although the representations and simulations of these mid-level clouds in global climate models are poor and under-predicted (Zhang et al., 2005), the balance of phases for these mixed-phase clouds (mid-level clouds) due to cloud-layer temperature or ice nuclei (IN) changes will certainly have a potentially large radiative impact in local regions (Sassen and Khvorostyanov, 2007). Thus, to quantify the feedback of an individual cloud type in these regions and document the local cloud climatology, related studies on mid-level clouds in these arid/semi-arid regions should focus on the impacts of dust aerosols on radiative effects and “cold rain processes” (Huang et al., 2006c; 2006d; Su et al., 2008; Wang et al., 2010).

Acknowledgments. This research was supported jointly supported by the National

Basic Research Program of China under No. 2013CB955802, No. 2012CB955301, the National Science Foundation of China under grant 41205015, the Developmental Program of Changjiang Scholarship and Innovative Research Team (IRT1018), the China 111 project (No. B13045) and the Fundamental Research Funds for the Central Universities (lzujbky-2013-105). We also would like to thank the CALIPSO, and CloudSat science teams for providing excellent and accessible data products that made this study possible.

References

- Ackerman, T. P., Liou, K.N., Valero, F. P. J., and Pfister, L.: Heating rates in tropical anvils, *J. Atmos. Sci.*, 45, 1606–1623, 1988.
- Barker, H.W.: Overlap of fractional cloud for radiation calculations in GCMs: a global analysis using CloudSat and CALIPSO data, *J. Geophys. Res.*, 113, D00A01, doi:10.1029/2007JD009677, 2008.
- Baum, B. A. and Wielicki, B. A.: Cirrus Cloud Retrieval Using Infrared Sounding Data: Multilevel Cloud Errors, *J. Appl. Meteor.*, 33, 107–117, 1994.
- Behrangi, A., Kubar, T., and Lambrigtsen, B. H.: Phenomenological Description of Tropical Clouds Using CloudSat Cloud Classification, *Mon. Weather. Rev.*, 140, 3235–3249, 2012.
- Betts, A. K. and Boers, R.: A cloudiness transition in a marine boundary layer, *J. Atmos. Sci.*, 47, 1480–1497, 1990.
- Cess, R. D., Potter, G. L., Blanchet, J. P., Boer, G. J., Del Genio, A. D., D'Águé M., Dymnikov, V., Galin, V., Gates, W. L., Ghan, S. J., Kiehl, J. T., Lacis, A. A., Le Treut, H., Li, Z. X., Liang, X.Z., McAvaney, B. J., Meleshko, V. P., Mitchell, J. F. B., Morcrette, J. J., Randall, D. A., Rikus, L., Roeckner, E., Royer, J. F., Schlese, U., Sheinin, D. A., Slingo, A., Sokolov, A. P., Taylor, K.E., Washington, W. M., Wetherald, R. T., Yagai, I., and Zhang, M. H.: Intercomparison and interpretation of climate feedback processes in 19 atmospheric general circulation models, *J. Geophys. Res.*, 95, 16601–16615, 1990.
- Chang, F. L. and Li, Z.: A new method for detection of cirrus overlapping- low clouds

and determination of their optical properties, *J. Atmos. Sci.*, 62, 3993–4009,
2005a.

Chang, F. L. and Li, Z.: A near global climatology of single-layer and overlapped
clouds and their optical properties retrieved from TERRA/MODIS data using a
new algorithm, *J. Clim.*, 18, 4752–4771, 2005b.

Chen, B., Huang, J., Minnis, P., Hu, Y., Yi, Y., Liu, Z., Zhang, D., and Wang, X.:
Detection of dust aerosol by combining CALIPSO active lidar and passive IIR
measurements, *Atmos. Chem. Phys.*, 10, 4241–4251, 2010.

Chen, C. and Cotton, W. R.: The physics of the marine stratocumulus- capped mixed
layer, *J. Atmos. Sci.*, 44, 2951–2977, 1987.

Chen, T., Rossow, W. B., and Zhang, Y.: Radiative Effects of Cloud-Type Variations,
J. Clim., 13, 264–286, 2000.

Choi, Y.S., Lindzen, R.S., Ho, C.H., and Kim, J.: Space observations of cold-cloud
phase change, *Proc. Natl Acad. Sci.*, 107, 11211–11216, 2010.

Doutriaux-Boucher, M. and Seze, G.: Significant changes between the ISCCP C and D
cloud climatologies, *Geophys. Res. Lett.*, 25, 4193–4196, 1998.

Eastman, R. and Warren, S. G.: A 39-Yr Survey of Cloud Changes from Land Stations
Worldwide 1971–2009: Long-Term Trends, Relation to Aerosols, and Expansion
of the Tropical Belt, *J. Clim.*, 26, 1286–1303, 2013.

Eastman, R., Warren, S. G., and Hahn, C. J.: Variations in Cloud Cover and Cloud
Types over the Ocean from Surface Observations, 1954–2008, *J. Clim.*, 24,
5914–5934, doi: 10.1175/2011JCLI3972.1, 2011.

Hagihara, Y., Okamoto, H., and Yoshida, R.: Development of a combined
CloudSat/CALIPSO cloud mask to show global cloud distribution, *J. Geophys.*
Res., 115, D00H33, doi:10.1029/2009JD012344, 2010.

Hahn, C. J., Rossow, W. B., and Warren, S. G.: ISCCP Cloud Properties Associated
with Standard Cloud Types Identified in Individual Surface Observations, *J.*
Clim., 14, 11–28, 2001.

Han, Q., Rossow, W. B., and Lacis, A. A.: Near-global survey of effective droplet
radii in liquid water clouds using ISCCP data, *J. Clim.*, 7, 465–497, 1994.

713 Hartmann, D. L., Ockert-Bell, M. E., and Michelsen, M.L.: The effect of cloud type
 714 on Earth's energy balance: global analysis, *J. Clim.*, 5, 1281–1304, 1992.

715 Haynes, J.M., Jakob, C., Rossow, W.B., Tselioudis, G., and Brown, J.: Major
 716 Characteristics of Southern Ocean Cloud Regimes and Their Effects on the
 717 Energy Budget, *J. Clim.*, 24, 5061–5080. doi: 10.1175/2011JCLI4052.1, 2011.

718 Haynes, J.M., Vonder-Haar, T.H., L'Ecuyer, T., Henderson, D.: Radiative heating
 719 characteristics of Earth's cloudy atmosphere from vertically resolved active
 720 sensors, *Geophys. Res. Lett.*, 40, 624–630, doi:10.1002/grl.50145, 2013.

721 Henderson, D.S., L'Ecuyer, T., Stephens, G., Partain, P., and Sekiguchi, M.: A
 722 multi-sensor perspective on the radiative impacts of clouds and aerosols, *J. Appl.*
 723 *Meteorol. Climatol.*, 52, 853–871, doi: 10.1175/JAMC-D-12-025.1, 2013.

724 Hogan, R. J. and Illingworth, A. J.: Deriving cloud overlap statistics from radar, *Q. J.*
 725 *Roy. Meteor. Soc.*, 128, 2903–2909, 2000.

726 Huang, J.P.: Analysis of ice water path retrieval errors over tropical ocean,
 727 *Advances in Atmospheric Sciences*, 23: 165–180, 2006a.

728 Huang, J. P., Minnis, P., and Lin, B.: Advanced retrievals of multilayered cloud
 729 properties using multispectral measurements, *J. Geophys. Res.*, 110, D15S18,
 730 doi:10.1029/2004JD005101, 2005.

731 Huang, J. P., Minnis, P., and Lin, B.: Determination of ice water path in ice-
 732 over-water cloud systems using combined MODIS and AMSR-E measurements,
 733 *Geophys. Res. Lett.*, 33, L21801, doi:10.1029/ 2006GL027038, 2006b.

734 Huang, J.P., Lin, B., Minnis, P., Wang, T., Wang, X., Hu, Y., Yi, Y., and Ayers, J.R.:
 735 Satellite-based assessment of possible dust aerosols semi-direct effect on cloud
 736 water path over East Asia, *Geophys. Res. Lett.*, 33, L19802, doi:
 737 10.1029/2006GL026561, 2006c.

738 Huang, J.P., Minnis, P., Lin, B., Wang, T., Yi, Y., Hu, Y., Sun-Mack, S., and Ayers,
 739 K.: Possible influences of Asian dust aerosols on cloud properties and radiative
 740 forcing observed from MODIS and CERES, *Geophys. Res. Lett.*, 33, L06824,
 741 doi: 10.1029/2005GL024724, 2006d.

742 Kato, S., Sun-Mack, S., Miller, W. F., Rose, F. G., Chen, Y., Minnis, P., and Wielicki,

- B. A.: Relationships among cloud occurrence frequency, overlap, and effective thickness derived from CALIPSO and CloudSat merged cloud vertical profiles, *J. Geophys. Res.*, 115, D00H28, doi:10.1029/2009JD012277, 2010.
- Klein, S. A. and Hartmann, D. L.: The seasonal cycle of low stratiform clouds, *J. Clim.*, 6, 1588–1606, 1993.
- L’Ecuyer, T.S., Wood, N., Haladay, T., and Stephens, G.L.: The impact of clouds on atmospheric heating based on the R04 CloudSat fluxes and heating rate dataset, *J. Geophys. Res.*, 113, D00A15, doi:10.1029/2008JD009951, 2008.
- Li, J., Yi, Y., Minnis, P., Huang, J., Yan, H., Ma, Y., Wang, W., and Ayers, k.: Radiative effect differences between multi-layered and single-layer clouds derived from CERES, CALIPSO, and CloudSat data, *J. Quant. Spectrosc. Radiat. Transf.*, 112, 361–375, 2011.
- Liang, X.Z., and Wu, X.: Evaluation of a GCM subgrid cloudradiation interaction parameterization using cloud-resolving model simulations, *Geophys. Res. Lett.*, 32, L06801, doi:10.1029/2004 GL022301, 2005.
- Liao, X., Rossow, W. B., and Rind, D.: Comparison between SAGE II and ISCCP high-level clouds. Part I: Global and zonal mean cloud amounts, *J. Geophys. Res.*, 100, 1121–1135, 1995.
- Luo, Y., Zhang, R., and Wang, H.: Comparing occurrences and vertical structures of hydrometeors between the eastern China and the Indian monsoon region using CloudSat/CALIPSO data, *J. Clim.*, 22, 1052–1064, 2009.
- Mace, G. G., and Benson-Troth, S.: Cloud-layer overlap characteristics derived from long-term cloud radar data, *J. Clim.*, 15, 2505–2515, 2002.
- Minnis, P., Yi, Y., Huang, J., and Ayers, J. K.: Relationships between radiosonde and RUC-2 meteorological conditions and cloud occurrence determined from ARM data, *J. Geophys. Res.*, 110, D23204, doi:10.1029/2005JD006005, 2005.
- Minnis, P., Huang, J., Lin, B., Yi, Y., Arduim, R., Fan, T.-F., Ayers, J. K., and Mace, G. G.: Ice cloud properties in ice-over-water cloud systems using Tropical Rainfall Measuring Mission (TRMM) visible and infrared scanner and TRMM Microwave Imager data, *J. Geophys. Res.*, 112, D06206, doi:

10.1029/2006JD007626, 2007.

Moran, J.M., Morgan, M.D., and Pauley, P.M.: *Meteorology: The Atmosphere and the Science of Weather*, Prentice Hall, New Jersey, 530pp, 1997.

Morcrette, J. J. and Jakob, C.: The response of the ECMWF model to changes in the cloud overlap assumption, *Mon. Weather. Rev.*, 128, 1707–1732, 2000.

Naud, C.M., DelGenio, A.D., Mace, G.G., Benson, S., Clothiaux, E.E., and Kollias, P.: Impact of dynamics and atmospheric state on cloud vertical overlap, *J. Clim.*, 21, 1758–1770, 2008.

Norris, J. R. and Leovy, C. B.: Interannual variability in stratiform cloudiness and sea surface temperature, *J. Clim.*, 7, 1915–1925, 1994.

Parker, S.P.: *Meteorology Source Book*. McGraw-Hill, New York, 304 pp, 1988.

Randall, D.A., Coakley, Jr. J.A., Fairall, C.W., Kropfli, R.A., and Lenschow, D.H.: Outlook for research on sub-tropical marine stratiform clouds, *Bull. Amer. Meteorol. Soc.*, 65, 1290–1301, 1984.

Rossow, W. B. and Schiffer, R. A.: ISCCP cloud data products, *B. Am. Meteorol. Soc.*, 72, 2–20, 1991.

Rossow, W. B. and Schiffer, R. A.: Advances in understanding clouds from ISCCP, *B. Am. Meteorol. Soc.*, 80, 2261–2286, 1999.

Sassen, K. and Cho, B. S.: Subvisual–thin cirrus lidar dataset for satellite verification and climatological research, *J. Appl. Meteor.*, 31, 1275–1285, 1992.

Sassen, K., and Khvorostyanov, V.I.: Microphysical and radiative properties of mixed phase altocumulus: a model evaluation of glaciation effects. *Atmos. Res.*, 84, 390–398, 2007.

Sassen, K. and Wang, Z.: Classifying clouds around the globe with the CloudSat radar: 1-year of results, *Geophys. Res. Lett.*, 35, L04805, doi:10.1029/2007GL032591, 2008.

Sassen, K., Wang, Z., and Liu, D.: Cirrus clouds and deep convection in the tropics: Insights from CALIPSO and CloudSat, *J. Geophys. Res.*, 114, D00H06, doi:10.1029/2009JD011916, 2009.

Stephens, G. L.: Cloud feedbacks in the climate system: a critical review, *J. Clim.*, 18,

237–273, 2005.

Stephens, G. L., Wood, N. B., and Gabriel, P. M.: An assessment of the parameterization of subgrid-scale cloud effects on radiative transfer: Part I. Vertical overlap, *J. Atmos. Sci.*, 61, 715–732, 2004.

Stephens, G.L., Vane, D.G., Boain, R.J., Mace, G.G., Sassen, K., Wang, Z., Illingworth, A.J., O'Connor, E.J., Rossow, W.B., Durden, S.L., Miller, S.D., Austin, R.T., Benedetti, A., Mitrescu, C., and CloudSat Science Team.: The CloudSat mission and the A-Train, A new dimension of space-based observations of clouds and precipitation, *B. Am. Meteorol. Soc.*, 83, 1771–1790, 2002.

Su, J., Huang, J., Fu, Q., Minnis, P., Ge, J., and Bi, J.: Estimation of Asian dust aerosol effect on cloud radiation forcing using Fu-Liou radiative model and CERES measurements, *Atmos. Chem. Phys.*, 8, 2763–2771, 2008.

Tian, L. and Curry, J. A.: Cloud overlap statistics, *J. Geophys. Res.*, 94, 9925–9935, 1989.

Trenberth, K.E., and Fasullo, J.T.: Simulation of present-day and twenty-first-century energy budgets of the southern oceans, *J. Clim.*, 23, 440–454, 2010.

Wang, L. and Dessler, A. E.: Instantaneous cloud overlap statistics in the tropical area revealed by ICESat/GLAS data, *Geophys. Res. Lett.*, 33, L15804, doi:10.1029/2005GL024350, 2006.

Wang, Z. and Sassen, K.: Cloud type and macrophysical property retrieval using multiple remote sensors, *J. Appl. Meteor.*, 40, 1665–1682, 2001.

Wang, W., Huang, J., Minnis, P., Hu, Y., Li, J., Huang, Z., Ayers, J. K., and Wang, T.: Dusty cloud properties and radiative forcing over dust source and downwind regions derived from A-Train data during the Pacific Dust Experiment, *J. Geophys. Res.*, 115, D00H35, doi: 10.1029/2010JD014109, 2010.

Warren, S. G., Eastman, R. M., and Hahn, C. J.: A survey of changes in cloud cover and cloud types over land from surface observations, 1971–96, *J. Clim.*, 20, 717–738, 2007.

Warren, S. G., Hahn, C. J., and London, J.: Simultaneous occurrence of different cloud

types, J. Clim. Appl. Meteorol., 24, 658–67, 1985.

Winker D. M., Hunt, W. H., and McGill, M. J.: Initial performance assessment of CALIOP, Geophys. Res. Lett., 34, L19803, doi:10.1029/2007GL030135, 2007.

World Meteorological Organization.: *International Cloud Atlas: Abridged atlas*, World Meteorological Organization, 62 pp., and 72 plates, Geneva, 1956.

Wylie, D.P., Eloranta, E., Spinhirne, J.D., and Palm, S.P.: A comparison of cloud cover statistics from the GLAS lidar with HIRS, J. Clim., 20, 4968–4981, doi:10.1175/JCLI4269.1, 2007.

Yu, R. C., Wang, B., and Zhou, T.: Climate effects of the deep continental stratus clouds generated by the Tibetan Plateau, J. Clim., 17, 2702–2713, 2004.

Yu, H., Remer, L. A., Chin, M., Bian, H., Tan, Q., Yuan, T., and Zhang, Y.: Aerosols from overseas rival domestic emissions over North America, Science, 337(6094), 566–569, doi:10.1126/science.1217576, 2012.

Yuan, T. and Oreopoulos, L.: On the global character of overlap between low and high clouds, Geophys. Res. Lett., 40, 5320–5326, doi:10.1002/grl.50871, 2013.

Zhang, D., Luo, T., Liu, D., and Wang, Z.: Spatial Scales of Altocumulus Clouds Observed with Collocated CALIPSO and CloudSat Measurements, Atmos. Res., 148, 58–69, doi: 10.1016/j.atmosres.2014.05.023, 2014.

Zhang, M. H., Lin, W. Y., Klein, S. A., Bacmeister, J. T., Bony, S., Cederwall, R. T., Del Genio, A.D., Hack, J. J., Loeb, N. G., Lohmann, U., Minnis, P., Musat, I., Pincus, R., Stier, P., Suarez, M. J., Webb, M. J., Wu, J. B., Xie, S. C., Yao, M. S., and Zhang, J. H.: Comparing clouds and 15 their seasonal variations in 10 atmospheric general circulation models with satellite measurements, J. Geophys. Res., 110, D15S02, doi:10.1029/2004JD005021, 2005.

Table 1. Globally averaged overlapping percentages of different cloud types over land and ocean during daytime.

	SL ^a	ML ^b	High	As	Ac	St/Sc	Cu	Ns	Deep	surface
High	8.8	14.5	3.7	2.5	4.3	3.2	2.8	1.0	0.4	Land
	8.8	16.4	4.1	2.2	3.5	5.2	3.5	1.2	0.3	Ocean
As	6.5	6.7	--	0.9	1.0	2.0	1.1	0.4	--	Land
	4.2	6.1	--	0.5	0.9	2.5	1.0	0.3	--	Ocean
Ac	5.3	7.0	--	0.01	1.1	0.9	1.1	0.04	--	Land
	3.1	6.4	--	0.01	0.8	1.5	1.0	0.08	--	Ocean
St/Sc	10.5	6.2	--	--	--	0.3	0.5	--	--	Land
	21.9	9.4	--	--	--	0.4	0.7	--	--	Ocean
Cu	3.9	5.1	--	--	--	0.1	0.3	--	--	Land
	6.6	5.9	--	--	--	0.2	0.3	--	--	Ocean
Ns	4.0	1.5	--	--	--	0.02	0.09	--	--	Land
	4.1	1.6	--	--	--	0.02	0.05	--	--	Ocean
Deep	0.8	0.4	--	--	--	--	--	--	--	Land
	0.8	0.3	--	--	--	--	--	--	--	Ocean

^aThe SL represents the single-layered cloud. ^bThe ML represents the multi-layered cloud. And, those boldfaced values indicated the overlapping percentages of different cloud types over ocean.

Table 2. Globally averaged overlapping percentages for different cloud types over land and ocean during nighttime.

	SL ^a	ML ^b	High	As	Ac	St/Sc	Cu	Ns	Deep	surface
High	12.0	17.4	5.5	3.2	6.6	2.6	1.8	1.3	0.3	Land
	8.8	20.8	4.7	2.3	5.0	7.6	4.4	1.3	0.3	Ocean
As	6.9	7.4	--	1.0	1.1	1.9	0.9	0.4	--	Land
	3.9	6.3	--	0.4	0.9	2.6	1.0	0.3	--	Ocean
Ac	4.6	8.5	--	0.01	1.2	0.7	0.6	0.05	--	Land
	3.1	8.1	--	0.01	1.0	1.9	1.2	0.08	--	Ocean
St/Sc	6.4	5.1	--	--	--	0.2	0.3	--	--	Land
	23.8	12.1	--	--	--	0.4	0.8	--	--	Ocean
Cu	2.0	3.4	--	--	--	0.1	0.2	--	--	Land
	5.9	6.9	--	--	--	0.2	0.4	--	--	Ocean
Ns	3.9	1.7	--	--	--	--	0.08	--	--	Land
	4.0	1.7	--	--	--	--	0.05	--	--	Ocean
Deep	0.8	0.3	--	--	--	--	--	--	--	Land
	0.9	0.3	--	--	--	--	--	--	--	Ocean

^aThe SL represents the single-layered cloud. ^bThe ML represents the multi-layered cloud. And, those boldfaced values indicated the overlapping percentages of different cloud types over ocean.

Table 3. Cloud fractions of different multilayered cloud types based on different overlap assumptions and observations during daytime. Here, $C_{overlap}$ and $C_1 \times C_2$ are the overlap cloud fraction from observations and overlap assumptions. “ a ” presents the overlap parameter.

Cloud type	C_{max}	C_{random}	C_{real}	$C_1 \times C_2$	$C_{overlap}$	R^a (W/m ²)	Diff. ^b	a
High+As	23.3 (25.2)	33.4 (32.9)	34.0 (33.3)	3.1 (2.6)	2.5 (2.2)	0.8 (0.8)	24.0% (18.2%)	-0.06 (-0.05)
High+Ac	23.3 (25.2)	32.7 (32.3)	31.3 (31.2)	2.9 (2.4)	4.3 (3.5)	-2.4 (-2.3)	-32.6% (-31.4%)	0.15 (0.15)
High+St/Sc	23.3 (31.3)	36.1 (48.6)	36.8 (51.3)	3.9 (7.9)	3.2 (5.2)	1.0 (3.9)	21.9% (51.9%)	-0.05 (-0.16)
High+Cu	23.3 (25.2)	30.2 (34.5)	29.5 (34.2)	2.1 (3.2)	2.8 (3.5)	-1.3 (-0.7)	-25.0% (-8.6%)	0.1 (0.03)
High+Ns	23.3 (25.2)	27.5 (29.5)	27.8 (29.7)	1.3 (1.4)	1.0 (1.2)	0.7 (0.5)	30.0% (16.7%)	-0.07 (-0.05)
High+Deep	23.3 (25.2)	24.2 (26.0)	24.1 (26.0)	0.3 (0.3)	0.4 (0.3)	-0.1 (0.0)	-25.0% (0.0%)	0.11 (0.0)
As+St/Sc	16.7 (31.3)	27.7 (38.4)	27.9 (39.1)	2.2 (3.2)	2.0 (2.5)	0.6 (2.5)	10.0% (28.0%)	-0.02 (-0.1)
As+Cu	13.2 (12.5)	21.0 (21.5)	21.1 (21.8)	1.2 (1.3)	1.1 (1.0)	0.4 (1.7)	9.1% (30.0%)	-0.01 (-0.03)
Ac+St/Sc	16.7 (31.3)	26.9 (37.8)	28.1 (39.3)	2.1 (3.0)	0.9 (1.5)	2.2 (3.9)	133.3% (100.0%)	-0.12 (-0.23)
Ac+Cu	12.3 (12.5)	20.2 (20.8)	20.2 (21.0)	1.1 (1.2)	1.1 (1.0)	0.0 (0.5)	0.0% (20.0%)	0.0 (-0.02)

^aCalculated from $(C_{random}-C_{real}) \times (\text{global mean cloud radiative effect of each cloud type})$. ^bCalculated from $(C_1 \times C_2 - C_{overlap}) / C_{overlap}$.

And, those boldfaced values in the brackets indicated the overlapping percentages of different cloud types over ocean surface. But for R^a , the values indicated the cloud radiative effect difference between real and random overlap at TOA and Surface (in the brackets), respectively. Here, only cloud radiative effects during daytime are considered.

Table 4. Cloud fractions of different multilayered cloud types based on different overlap assumptions and observations during nighttime. Here, $C_{overlap}$ and $C_1 \times C_2$ are the overlap cloud fraction from observations and overlap assumptions. “ a ” presents the overlap parameter.

Cloud type	C_{max}	C_{random}	C_{real}	$C_1 \times C_2$	$C_{overlap}$	$R^a (W/m^2)$	Diff. ^b	a
High+As	29.4 (29.6)	39.5 (36.8)	40.5 (37.5)	4.2 (3.0)	3.2 (2.3)	- -	31.3% (30.4%)	-0.1 (-0.1)
High+Ac	29.4 (29.6)	38.6 (37.5)	35.9 (35.8)	3.9 (3.3)	6.6 (5.0)	- -	-40.9% (-34.0%)	0.29 (0.22)
High+St/Sc	29.4 (35.9)	37.5 (54.9)	38.3 (57.9)	3.4 (10.6)	2.6 (7.6)	- -	30.8% (39.5%)	-0.1 (-0.16)
High+Cu	29.4 (29.6)	33.2 (38.6)	33.0 (38.0)	1.6 (3.8)	1.8 (4.4)	- -	-11.1% (-13.6%)	0.05 (0.07)
High+Ns	29.4 (29.6)	33.4 (33.6)	33.7 (34.0)	1.6 (1.7)	1.3 (1.3)	- -	23.1% (30.8%)	-0.08 (-0.1)
High+Deep	29.4 (29.6)	30.2 (30.4)	30.2 (30.5)	0.3 (0.4)	0.3 (0.3)	- -	0.0% (33.3%)	0.0 (-0.13)
As+St/Sc	14.3 (35.9)	24.2 (42.4)	23.9 (43.5)	1.6 (3.7)	1.9 (2.6)	- -	-15.8% (42.3%)	0.03 (-0.17)
As+Cu	14.3 (12.8)	18.9 (21.7)	18.8 (22.0)	0.8 (1.3)	0.9 (1.0)	- -	-11.1% (30.0%)	0.02 (-0.03)
Ac+St/Sc	13.1 (35.9)	23.1 (43.1)	23.9 (45.2)	1.5 (4.0)	0.7 (1.9)	- -	114.3% (110.5%)	-0.08 (-0.29)
Ac+Cu	13.1 (12.8)	17.8 (22.6)	17.9 (22.8)	0.7 (1.4)	0.6 (1.2)	- -	16.7% (16.7%)	-0.02 (-0.02)

^aCalculated from $(C_{random} - C_{real}) \times (\text{global mean cloud radiative effect of each cloud type})$. ^bCalculated from $(C_1 \times C_2 - C_{overlap}) / C_{overlap}$.
And, those boldfaced values in the brackets indicated the overlapping percentages of different cloud types over ocean surface. But for R^a , the values indicated the cloud radiative effect difference between real and random overlap at TOA and Surface (in the brackets), respectively. Here, only cloud radiative effects during daytime are considered.

956

957 **Figure captions**

958 Figure 1. (a) The global distribution ($2^{\circ} \times 2^{\circ}$ grid boxes) of annually averaged
959 multilayered cloud fraction. (b) The zonal distributions of seasonal averaged
960 multilayered cloud fraction.

961 Figure 2. Zonal distributions of annual most frequently occurring multilayered cloud
962 types based on the 2B-CLDCLASS-Lidar product.

963 Figure 3. The global distributions of (a) the annual mean dominant cloud types and (b)
964 the corresponding cloud fractions. And, the global distributions of (c) the annual
965 mean dominant multiple cloud types and (d) the corresponding cloud amounts.

966 Figure 4. (a)-(b):The zonal variation of cloud along-track horizontal scales for these
967 multilayered cloud systems and (c)-(d): their probability distribution.

968 Figure 5. (a)-(d):The zonal distributions of cloud radiative effect and weighted cloud
969 radiative effect for different multilayered cloud systems at the top of atmosphere
970 (TOA) during daytime.

971 Figure 6. Same with Figure5, but at the surface during the daytime.

972 Figure 7. The global average cloud radiative effect and weighted cloud radiative effect
973 for different multilayered cloud types at TOA and surface only during daytime.
974 The gray line presents the global average frequency of occurrence of each cloud
975 type only during daytime (that is, weights). The total weighted cloud radiative
976 effects of whole multilayered cloud system are also showed in the figure 7c and
977 7d. TOA (-22.7 W/m^2); Surface (-27.1 W/m^2).

978 Figure 8. (a)-(b): The zonal distributions of the relative difference for different
979 multilayered cloud types and the cumulative relative difference of all
980 multilayered cloud types (gray line). (c)-(d): The zonal distributions of the
981 overlap parameter for different multilayered cloud types and the cumulative
982 overlap parameter of all multilayered cloud types (gray line).

983 Figure 9. The global distributions of (a) the cumulative relative difference and (b) the
984 cumulative overlap parameter of all multilayered cloud types.

985

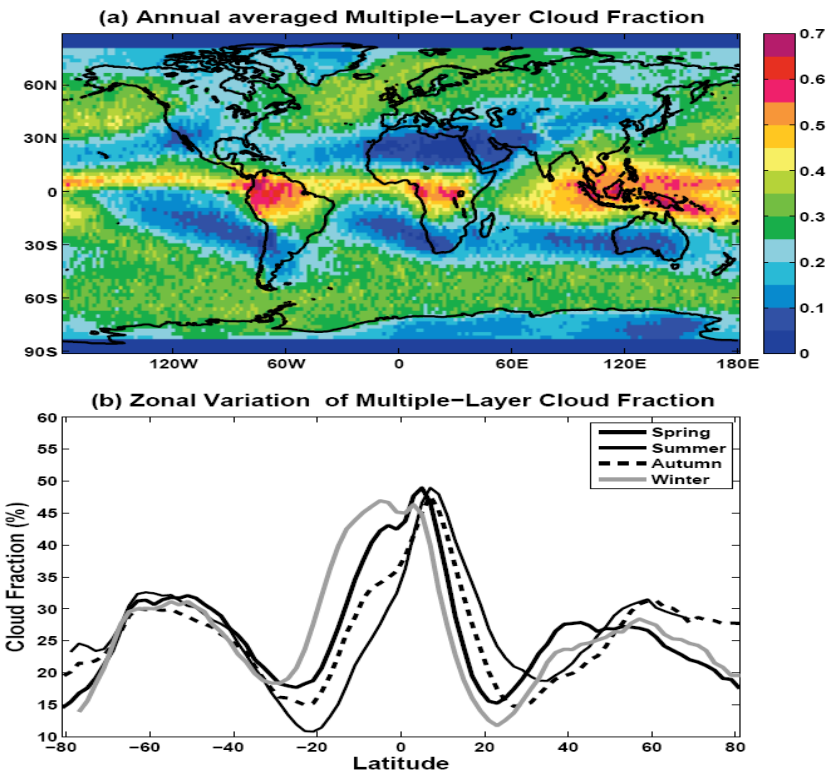


Figure 1. (a) The global distribution ($2^{\circ}\times 2^{\circ}$ grid boxes) of annually averaged multilayered cloud fraction. (b) The zonal distributions of seasonal averaged multilayered cloud fraction.

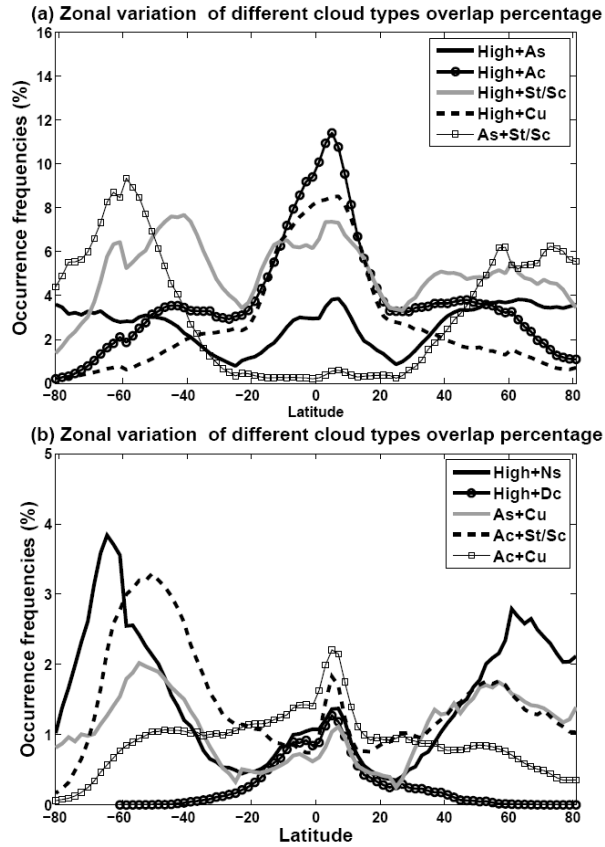
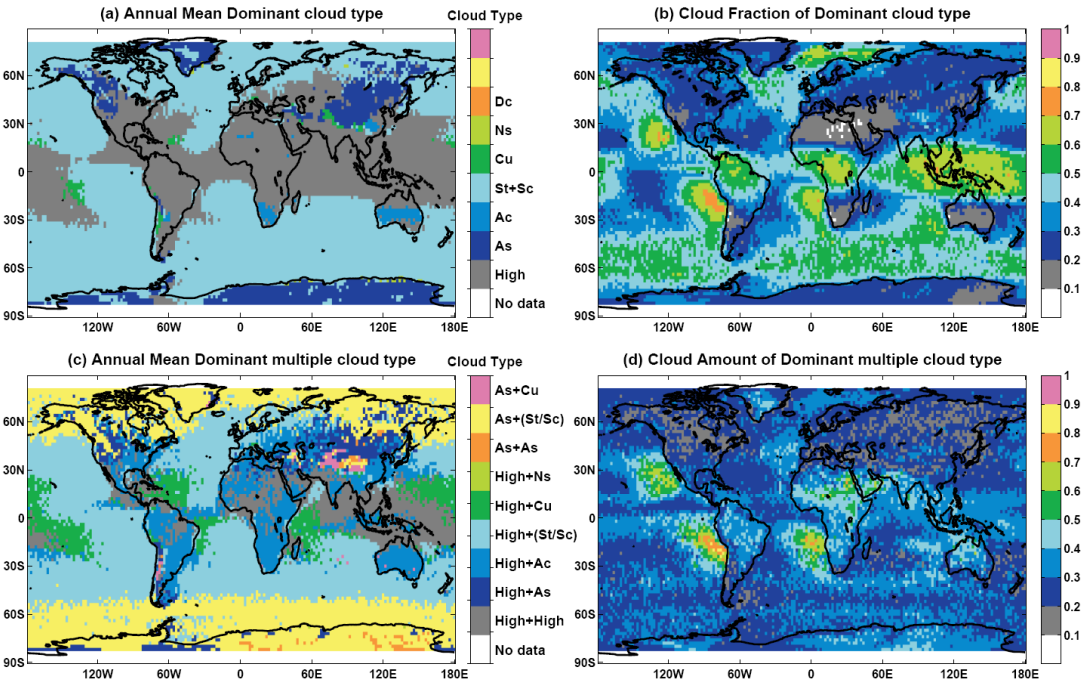


Figure 2. Zonal distributions of annual most frequently occurring multilayered cloud types based on the 2B-CLDCLASS-Lidar product.



1022

1023

1024

1025

1026

1027

1028

1029

1030

1031

1032

1033

1034

1035

1036

1037

1038

1039

Figure 3. The global distributions of (a) the annual mean dominant cloud types and (b) the corresponding cloud fractions. And, the global distributions of (c) the annual mean dominant multiple cloud types and (d) the corresponding cloud amounts.

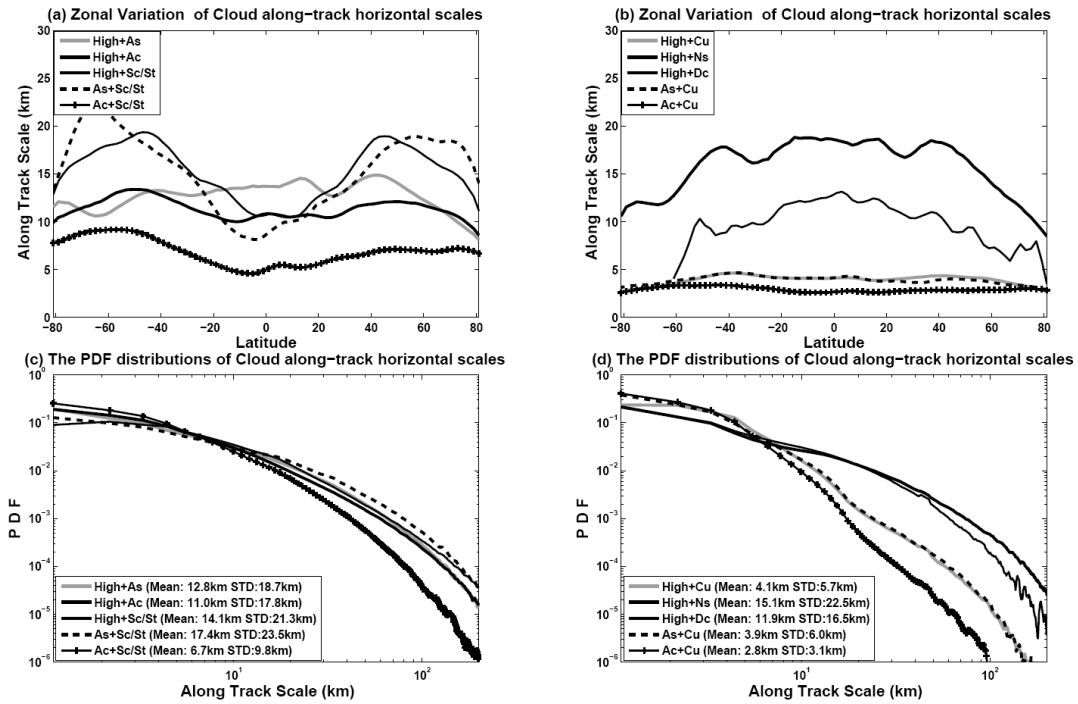
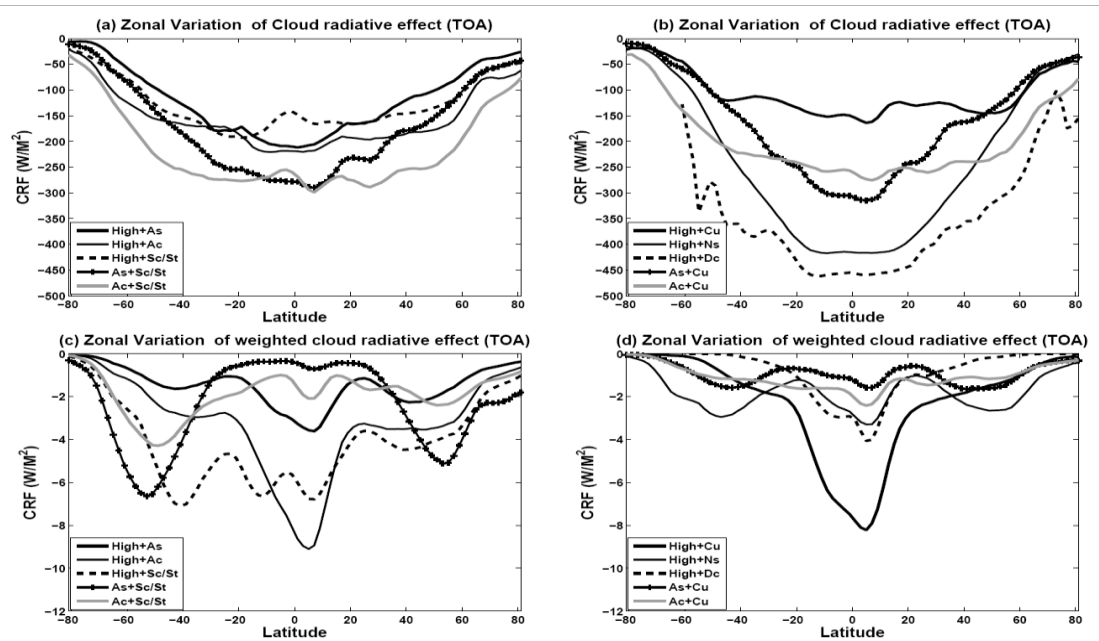


Figure 4. (a)-(b):The zonal variation of cloud along-track horizontal scales for these multilayered cloud systems and (c)-(d): their probability distribution.



1060

1061 Figure 5. (a)-(d):The zonal distributions of cloud radiative effect and weighted cloud
 1062 radiative effect for different multilayered cloud systems at the top of atmosphere
 1063 (TOA) during daytime.

1064

1065

1066

1067

1068

1069

1070

1071

1072

1073

1074

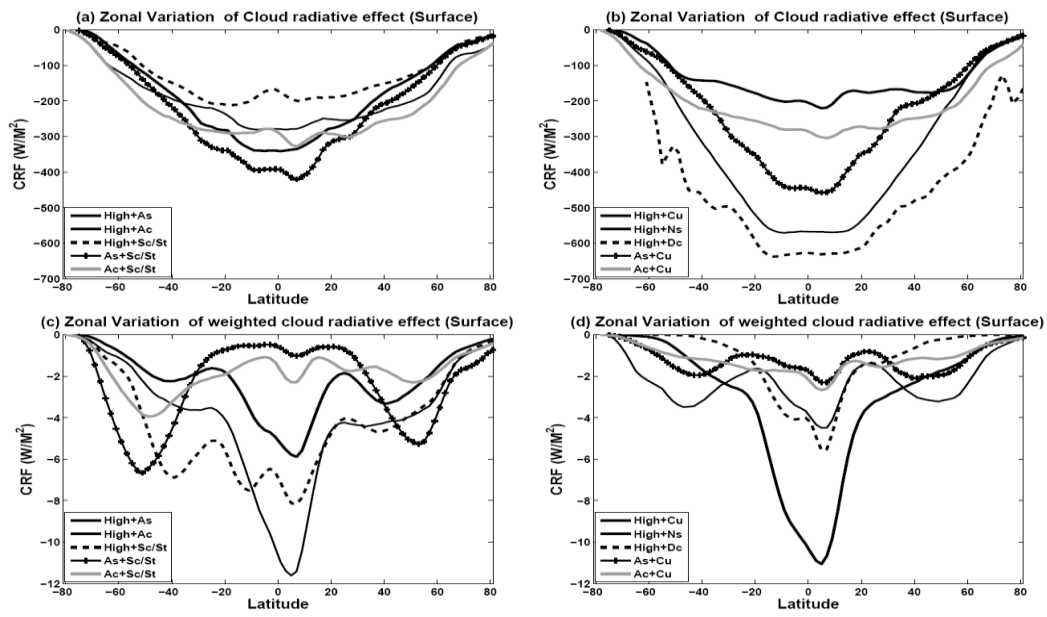
1075

1076

1077

1078

1079



1080

1081 Figure 6. Same with Figure5, but at the surface during the daytime.

1082

1083

1084

1085

1086

1087

1088

1089

1090

1091

1092

1093

1094

1095

1096

1097

1098

1099

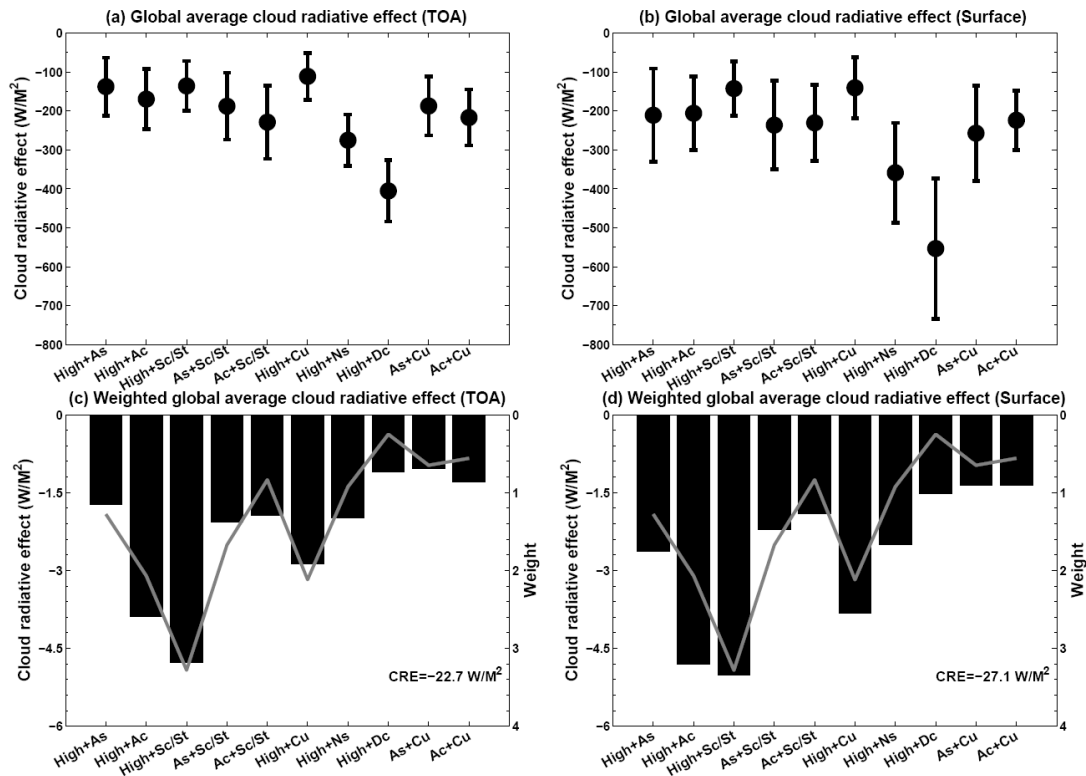
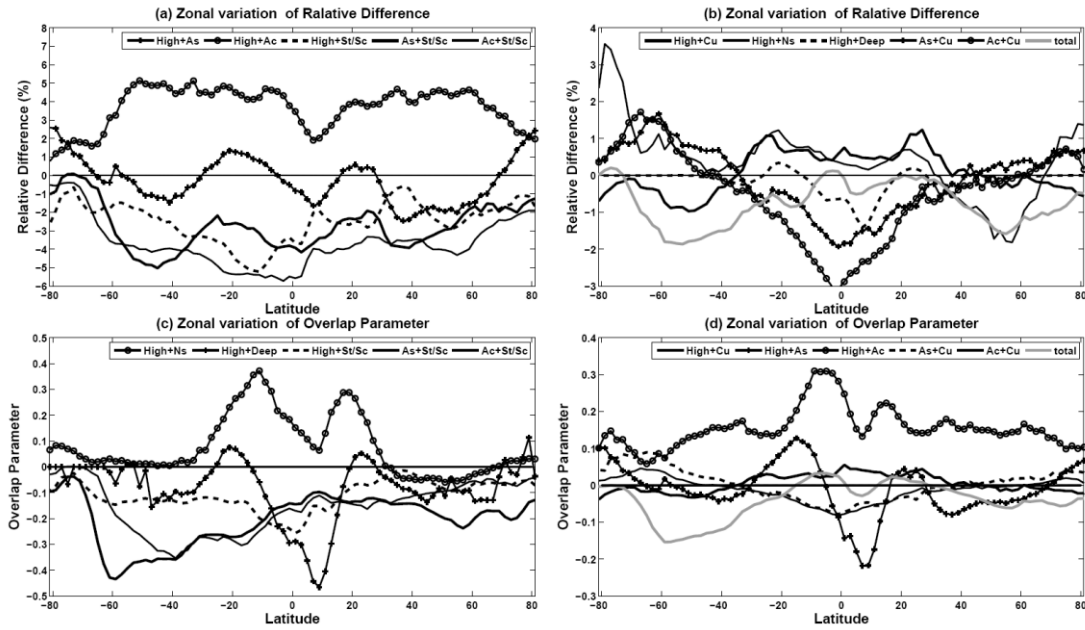


Figure 7. The global average cloud radiative effect and weighted cloud radiative effect for different multilayered cloud types at TOA and surface only during daytime. The gray line presents the global average frequency of occurrence of each cloud type only during daytime (that is, weights). The total weighted cloud radiative effects of whole multilayered cloud system are also showed in the figure 7c and 7d. TOA (-22.7 W/m²); Surface (-27.1 W/m²).

1118



1119

1120 Figure 8. (a)-(b): The zonal distributions of the relative difference for different
 1121 multilayered cloud types and the cumulative relative difference of all multilayered
 1122 cloud types (gray line). (c)-(d): The zonal distributions of the overlap parameter for
 1123 different multilayered cloud types and the cumulative overlap parameter of all
 1124 multilayered cloud types (gray line).

1125

1126

1127

1128

1129

1130

1131

1132

1133

1134

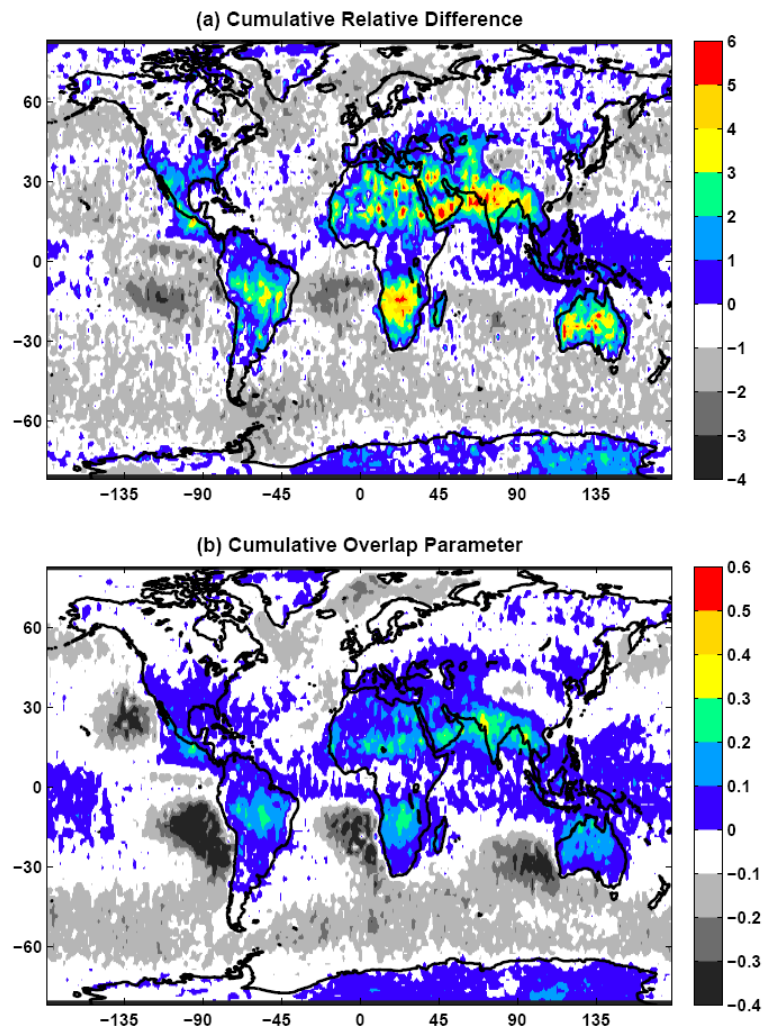
1135

1136

1137

1138

1139



1140

1141 Figure 9. The global distributions of (a) the cumulative relative difference and (b) the
1142 cumulative overlap parameter of all multilayered cloud types.